CrossMark

ORIGINAL PAPER

Protoporphyrin IX conjugated bacterial cellulose via diamide spacer arms with specific antibacterial photodynamic inactivation against *Escherichia coli*

Jiancheng Dong · Reza A. Ghiladi · Qingqing Wang · Yibing Cai · Qufu Wei

Abstract Herein, protoporphyrin IX (PPIX) was covalently grafted onto a bacterial cellulose (BC) surface via three diamine spacer arms with different chain lengths. The obtained materials were characterized by spectroscopic (infrared, Raman, UV–Vis diffuse reflectance, electron paramagnetic and fluorescence) and physical (elemental, gravimetric) methods. Antibacterial efficacy was evaluated against *Staphylococcus aureus* and *Escherichia coli*, and the PPIX supported BC surface exhibited specific antibacterial photodynamic inactivation against *E. coli*. The 1,2-bis(2-aminoethoxy)ethane aminated BC immobilized the maximal amount of PPIX, and the resulting photosensitive surface achieved a 99.999% (1st cycle) inactivation efficiency against *E. coli*, but relatively low efficiency against *S. aureus*. A mechanism of Gram negative bacterial inactivation was proposed as the positively charged PPIX-conjugated BC surface coupled with sufficient $^1O_2$ generation. Though the reusability of the as-fabricated materials needs to be further enhanced, this work provides a potent strategy for efficient photodynamic inactivation against Gram negative bacteria using neutral photosensitizers.

Keywords Protoporphyrin IX · Bacterial cellulose · aPDI · Specific antibacterial effect · *Escherichia coli*

A4 J. Dong · Q. Wang · Y. Cai · Q. Wei (✉)
A5 Key Laboratory of Eco-Textiles, Ministry of Education,
A6 Jiangnan University, Wuxi 214122, China
A7 e-mail: qfwei@jiangnan.edu.cn

A8 J. Dong
A9 e-mail: Jesse_D@outlook.com

A10 Q. Wang
A11 e-mail: qqwang@jiangnan.edu.cn

A12 Y. Cai
A13 e-mail: yibiingcai@163.com

A14 R. A. Ghiladi
A15 Department of Chemistry, North Carolina State
A16 University, Raleigh, NC 27695, USA
A17 e-mail: Reza_Ghiladi@NCSU.edu

Introduction

Owing to the increase in multidrug-resistant organisms from the overuse of antibiotics, the prevention of pathogenic infections is becoming a major medical and societal issue necessitating research efforts that focus on new antibacterial therapies and mechanisms of action. One such approach, antimicrobial photodynamic inactivation (aPDI), is a promising alternative or complementary method for preventing infections caused by microorganisms, including bacteria, viruses, fungi and protozoa (Jori et al. 2011). Commonly, aPDI employs photosensitizers that when

activated by visible or infrared light illumination in the presence of oxygen generates reactive oxygen species (ROS), including free radicals (Type I reaction) and singlet oxygen (Type II reaction; Abrahamse and Hamblin 2016), which lead to the inactivation of microorganisms. Owing to the diffusibility of these ROS, the photosensitizers do not have to come into contact with bacteria to be effective for photoinactivation (Dahl et al. 1987), while resistance to ROS as biocidal agents produced by aPDI is considered unlikely. As such, the immobilization of photosensitizers onto materials, including nanoscale scaffolds, has been arousing extensive research interests for their potential applicability as broad spectrum anti-infective platforms.

Photoantimicrobial conjugates have been obtained by incorporating photosensitizers onto a variety of scaffolds of various dimensions, including fabrics (Castriciano et al. 2017; Rahimi et al. 2016; Ringot et al. 2011), artificial polymers (Stanley et al. 2016), and even antimicrobial peptides (Johnson et al. 2016; Liu et al. 2012) for targeting and photoinactivation of pathogens. Generally, fabrics and nonwovens consist of micron-scale fibers, however, as the diffusion of $^1O_2$ is limited to hundreds of nanometers (Dahl et al. 1987), the blocking of $^1O_2$ by the fibers may lead to inefficient aPDI. Immobilization of photosensitizers on nanosurfaces overcomes the shortcoming of limited $^1O_2$ diffusion (Shrestha et al. 2014), yet properties like hydrophilicity (Henke et al. 2014) (Dolanský et al. 2015), specific surface area and surface charging (Vallapa et al. 2011) (Gottenbos et al. 2003) also play important roles in photodynamic inactivation. While photosensitizers immobilized on artificial nanofibers have been the subject of several recent studies, the use of natural biopolymers has been more limited.

Bacterial cellulose (BC), biosynthesized by *Acetobacter xylinum*, is a naturally produced nanomaterial with inherent biocompatibility, superhydrophilicity, large specific surface area and high mechanical strength (Lv et al. 2016), which enables BC to be a desirable nanocarrier for photosensitizers. In addition, the eco-friendly BC provides an inexpensive and renewable material that is easily scalable. Thus, towards our objective of creating anti-infective platforms from renewable nanoscaffolds based upon aPDI, here we present the covalent grafting of a neutral photosensitizer, protoporphyrin IX (PPIX), onto the surface of BC using diamine spacer arms with different chain lengths. Our hypothesis was that by employing variable chain length spacer arms, we could circumvent the potential for steric hindrance between the PPIX macrocycle (as photosensitizer) and BC (as scaffold), thereby increasing antimicrobial efficacy. Specifically, three diamine spacers with backbone chain lengths of 4 (EDA), 10 [1,2-bis(2-aminoethoxy)ethane] and 14 atoms [1,4-bis(3-amino-propoxy)butane] were applied to analyze their influence on BC surface functionalization and subsequent photoinactivation performance. The obtained materials were characterized by spectroscopic (infrared, Raman, diffuse reflectance UV–Vis, fluorescence) and physical (elemental, thermal gravimetric) methods. Photo-oxidation studies of external substrates and electron paramagnetic spectroscopy were used to quantify the relative amount of singlet oxygen produced as a function of the diamine spacer units. Antibacterial efficacy was evaluated against both *Staphylococcus aureus* and *Escherichia coli* as a function of the diamine spacer unit, and the reusability of the material was explored through repetitive aPDI assays. As will be shown, although the efficacy against *S. aureus* was more limited, the PPIX-grafted BC membranes achieved a 99.999% inactivation efficiency against *E. coli*, demonstrating that this work provides a potent strategy for the efficient photodynamic inactivation of G$^-$ bacteria using a photosensitizer and nanoscaffold that are both derived from natural sources.

Experimental section

Materials

Pure bacterial cellulose was obtained after an alkali cleaning process (Li et al. 2017). Sodium periodate, dimethylsulfoxide (DMSO), acetic acid and ethylenediamine (EDA) were purchased from Sinopharm Chemical Reagent Co., Ltd. 1,2-bis(2-aminoethoxy)ethane, 1,4-bis(3-aminopropoxy)butane, sodium cyanoborohydride, protoporphyrin IX, carbonyldiimidazole (CDI), 2,2,6,6-tetramethyl-4-piperidone (TEMPONE) and 1,4-diazabicyclo[2.2.2]octane (DABCO) were obtained from Sigma-Aldrich (China). *S. aureus* (ATCC-6538) and *E. coli* (ATCC-8099) were from Shanghai Xiejiu Bio-Tech Co., Ltd. All chemicals were used as received.

Periodate oxidation of bacterial cellulose

Oxidized bacterial cellulose (OBC) was prepared by sodium periodate oxidation in aqueous solution. Briefly, 500 g pristine BC membranes were immersed into 1000 mL of 0.4 M sodium periodate solution, and the mixture was gently shaken for 4 h at 37 °C in a photophobic beaker, followed by immersion in 1,2-ethanediol overnight to remove excess periodate. 1,2-Ethanediol was removed by deionized water, and the OBC was freeze-dried for next steps.

Surface amination by the 'one pot, two steps' method

Three linear diamine compounds were incorporated onto OBC membranes by the 'one pot, two steps' method. Typically, 200 mg of OBC membranes were immersed in a solution that consisted of 50 mmol EDA and 50 mL DMSO, and was adjusted by acetic acid to pH 6.0. The mixture was gently shaken for 12 h at 37 °C, and then 60 mmol of sodium cyanoborohydride was added into the solution, and the reaction continued for 24 h under the same conditions. The aminated membranes were subsequently washed with DMSO (30 mL × 3) and deionized water (30 mL × 5), and then freeze-dried. The surface aminated BC membranes will henceforth be generally referred to as BC-spacer-NH_2, whereas those functionalized specifically with EDA, 1,2-bis(2-aminoethoxy)ethane, and 1,4-bis(3-aminopropoxy)butane are assigned as BC-EDA-NH_2, BC-10-NH_2, and BC-14-NH_2, respectively.

Immobilization of PPIX onto aminated BC membranes

To activate the carboxylic acid groups of the PPIX macrocycle, a mixture of 0.3 mmol of CDI and 0.15 mmol PPIX in 50 mL DMSO was vigorously stirred for 4 h at 40 °C. Then, 200 mg of the BC-spacer-NH_2 membranes was added, and the reaction continued for 24 h. Extensive washing of the PPIX immobilized membranes with DMSO (30 mL × 4) followed to remove unreacted reagents. After that, the resulting membranes were vacuum-dried at 40 °C for 6 h. The resulting PPIX-grafted BC membranes will be generally referred to as BC-spacer-PPIX, and the specific different diamine spacer lengths,

ethylenediamine, 1,2-bis(2-aminoethoxy)ethane, 1,4-bis(3-aminopropoxy)butane, are referred to as BC-EDA-PPIX, BC-10-PPIX and BC-14-PPIX, respectively (Scheme 1).

Characterization

Scanning electron microscope (SEM) images were obtained using a Hitachi SU1510 (Japan) at 5.0 kV. Chemical structures of all samples were analyzed by Fourier transform infrared spectroscopy (ATR-FTIR, Nicolet Nexus, USA) and Raman microscope (Renishaw RM1000, Britain) with excitation at 514 nm. UV–Vis diffuse reflectance (DRUV) spectra were collected on a Shimadzu UV-3600 (Japan) spectrophotometer with barium sulfate as the background utilizing the wavelength range of 300–800 nm. Fluorescence imaging was recorded on a Hitachi F-7000 spectrometer (Japan). Elemental analyses were conducted by Vario Micro Cube elemental analyzer (Germany) and X-ray photoelectron spectroscopy (XPS, Thermo Scientific Escalab, USA) with monochromatized Al K_α radiation. Thermal gravimetric analysis (TGA) was carried out on a TA Q500 (USA) ramping 10 °C/min under N_2 purging. Unless otherwise stated, BC-10-NH_2 and BC-10-PPIX were chosen as the typical samples for the aforementioned characterization methods.

Photosensitization of external substrates and model bacteria

All photo-oxidation and photoinactivation experiments were performed using a Xenon lamp (500 W) equipped with a long-pass filter ($\lambda \geq 420$ nm), and the distance between all samples and the lamp center was fixed at 20 cm. An electric fan was used to prevent heating of the 24-well plate.

Photosensitization of external substrates

BC-spacer-PPIX membranes were cut into circular pieces with a diameter of 1.5 cm using a tablet cutter. A piece of circular membrane was immersed into a 10 mL beaker which contained 6 mL of 0.05 M potassium iodide solution, the beaker was covered with transparent polyethylene (PE) film to prevent water evaporation, and then the solution was illuminated with vigorous magnetic stirring. The UV
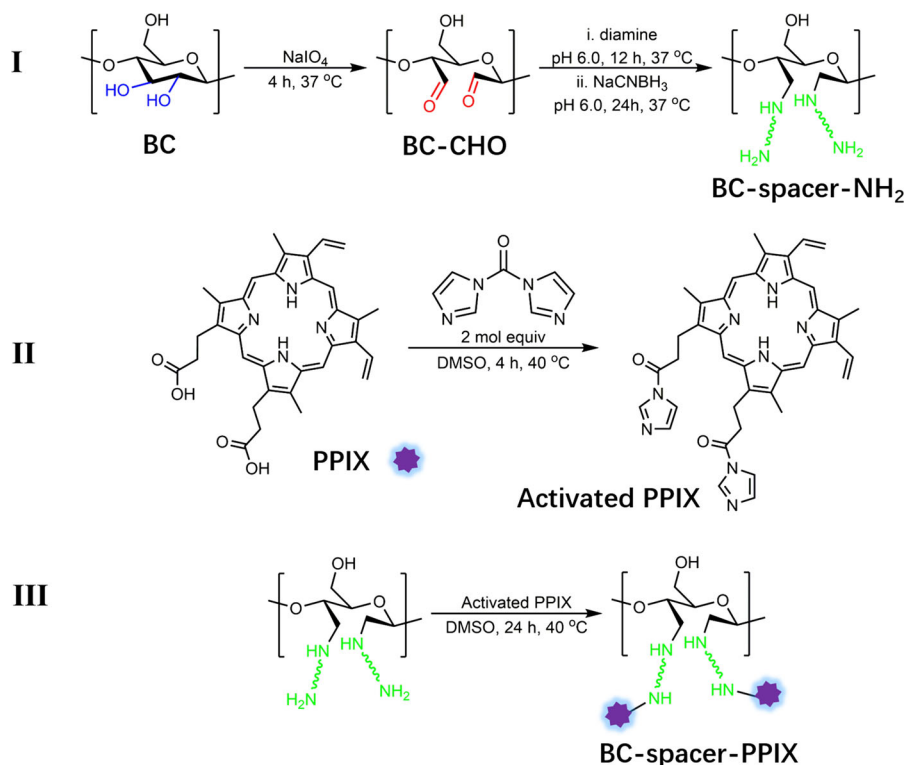
Scheme 1 Surface functionalization and PPIX immobilization yielding BC-spacer-PPIX nanofibrous membranes (Zhu and Sun 2012)

absorbance at 287 nm was recorded at regular intervals and compared to a blank solution that was stored in the dark. The oxidation mechanism (Wen et al. 2017) is shown in Eq. 1.

$$^1O_2 + 3I^- + 2H_2O \rightarrow I_3^- + 2H_2O_2 \qquad (1)$$
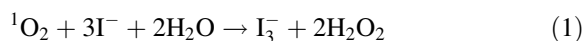
Antibacterial photoinactivation of model bacteria

Photoinactivation studies employing the model bacteria *S. aureus* and *E. coli* were performed in triplicate as previously described (Carpenter et al. 2012, 2015; Stanley et al. 2016). Briefly, three samples of BC-spacer-PPIX membranes (1.5 cm diam.) were individually placed into adjacent wells of two identically prepared 24-well plates. A 100 μL aliquot of PBS containing 10^7–10^8 CFU of bacteria was added to each of the three wells per plate. Once inoculated, the 24-well plate was illuminated for 30 min with a Xenon lamp ($\lambda \geq 420$ nm), while the other 24-well plate was kept without illumination as a dark control. Following illumination, 0.9 mL of sterile PBS was added to each well in both the illuminated and the dark control

plates, and the plates were vigorously vortexed for 5 min to re-suspend the bacteria. Then each well was 1:10 serially diluted (100 μL in 0.9 mL aliquots of PBS) five times, and 10 μL from the undiluted and each diluted well were separately plated in columns on gridded six column square TSA (for *S. aureus*) or LB (for *E. coli*) agar plates, followed by 12 h of dark incubation at 37 °C. Pristine BC was evaluated in the same method as a PPIX-free control, and a material-free control (24-well plate without sample membranes) was used to calculate the bacteria survival rate. The survival rate was determined by the ratio of CFU/mL of the illuminated or dark-control plates versus that of the material-free control. The minimum detection limit was 100 CFU/well (based on the plated 10 μL aliquot from the 1 mL undiluted well), and the detection limit range of bacteria survival is 0.01–0.001%.

Electron paramagnetic resonance (EPR) analysis

Detection of singlet oxygen followed the procedure of Lion and Moan (Moan and Wold 1979). Briefly, the

TEMPONE trapped EPR spectra of the BC-10-PPIX membrane in D_2O solution were obtained using a Bruker EMXplus-10/12 spectrometer at room temperature, which was operated at X-field with a center field at 3360 G and a sweep width of 70 G. The microwave frequency was 9.172 GHz, the power was 10 mW, the sweep time of the signal channel was 0.128 s, and a received gain of 8000 was employed. A 1.5 cm diameter sample of the BC-10-PPIX membrane was added into 3 mL oxygen saturated D_2O solution containing 1 mM TEMPONE, and illuminated for 30 min using a Xenon lamp ($\lambda \geq 420$ nm) with vigorous magnetic stirring. The resulting solution was transferred into an EPR capillary tube, which was then fixed in the resonant cavity of the spectrometer. The references for singlet oxygen quenching using DABCO and blank (pure D_2O) groups were also carried out to further confirm the production of singlet oxygen.

Results and discussion

Morphology observation

The morphologies of the nanofibrous membrane surfaces were examined by SEM. The freeze-dried pristine bacterial cellulose (Fig. 1a) displayed a typical three-dimensional structure of web-shaped microfibrils which were randomly distributed with unspecific orientation. During freeze-drying, ice encapsulated in the entangled nanofibrils sublimed directly to form a pore geometry (Wu and Meredith 2014), and the measured BET surface area reached 52.9091 m^2/g. Conversely, the PPIX-immobilized BC-10-PPIX membrane surface exhibited a compact network with the fiber bundle closely tangled together (Fig. 1b), likely due to either thermal drying (Fernandes et al. 2009) and/or chemical treatments as compared to the pristine BC. Upon periodate oxidation, the ordered packing of glucopyranose was broken (Kim et al. 2000) resulting in a decrease of water holding capacity (Figure S1), and subsequent thermal drying led to a collapsed fibrous network (17.4061 m^2/g), with subsequent treatments exacerbating the network shrinkage.

Chemical structure analysis

ATR-FTIR spectroscopic characterization

A strategy employing variable chain length spacer arms was used to circumvent the potential for steric hindrance between the PPIX macrocycle (as photosensitizer) and OBC (as scaffold; Krouit et al. 2009). In this work, three diamine spacers with backbone chain lengths of 4 (EDA), 10 [1,2-bis(2-aminoethoxy)ethane] and 14 atoms [1,4-bis(3-aminopropoxy)butane] were applied to analyze their influence on OBC surface functionalization and subsequent photoinactivation performance. The obtained membranes were characterized via ATR-FTIR spectroscopy to investigate changes in chemical structure during oxidation and amination (Fig. 2a). Upon treatment with sodium periodate, a new stretch at 1730 cm^{-1} was assigned to the C=O stretching vibration in OBC, while the band at $\sim$ 880 cm^{-1} was ascribed to the formation of hemiacetal bonds (Li et al. 2011). After amination, several new features appeared when compared with that of OBC membrane: (1) for all three aminated membranes, new bands appeared at 1569 cm^{-1} and were attributed to N–H bending (Zhu and Sun 2012),
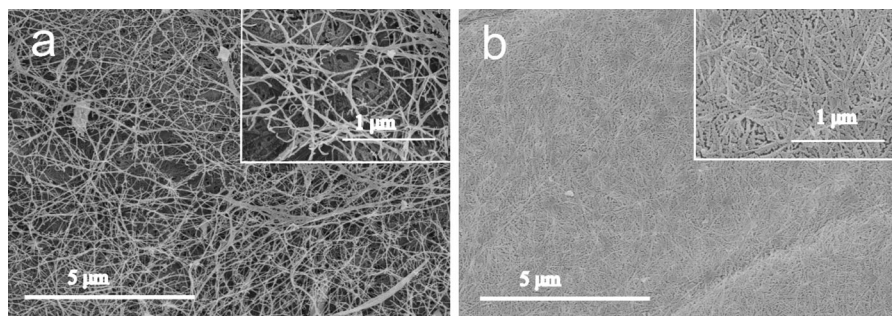

Fig. 1 SEM images of **a** pristine bacterial cellulose and **b** PPIX-immobilized BC-10-PPIX membranes
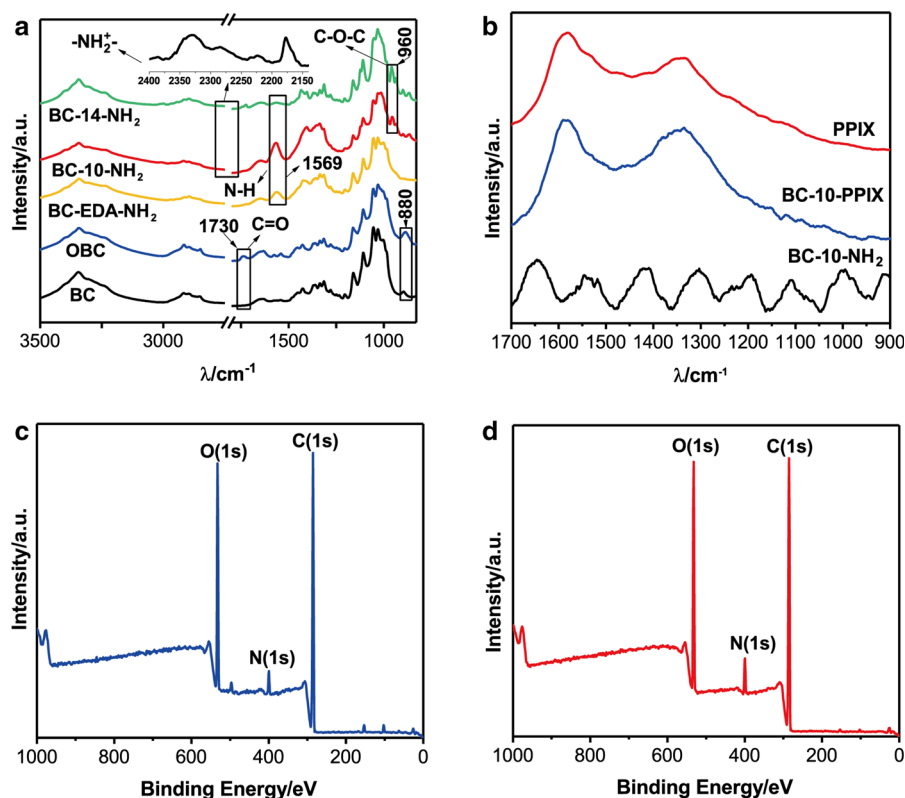
Fig. 2 ATR-FTIR spectra of **a** BC, OBC and BC-spacer-NH₂, **b** resonance Raman spectra of free PPIX, BC-10-NH₂, and BC-10-PPIX, and XPS survey scans of **c** BC-10-NH₂ and **d** BC-10-PPIX

consistent with a covalent amide linkage between the membrane surface and diamine spacers; (2) new features were observed at ~ 960 cm^{-1}, and were assigned to C–O–C stretching from the ether groups of the 10- and 14-atoms spacers; and (3) the broad peaks around 2150–2400 cm^{-1} are likely ascribed to N–H (–NH$_2^+$–) stretching (Onem and Nadaroglu 2014).

While the ATR-FTIR spectra demonstrated the covalent attachment of the spacer units onto the OBC surface, elemental analysis was carried out to assess

the total amount of each spacer (Table 1). The diamine loading values were 0.389, 1.775 and 0.425 mmol/g for BC-EDA-NH₂, BC-10-NH₂ and BC-14-NH₂, respectively. In comparison to the excellent loading of BC-10-NH₂ (degree of substitution, DS = 0.39) we surmise that the lower loading of BC-14-NH₂ (DS = 0.075) may be due to the inter- or intramolecular entanglement of the long chains that could lead to a lower reactivity of this spacer unit, whereas the low loading of the shorter EDA (DS = 0.065) may be due

Table 1 Diamine and PPIX loading values of the different BC-spacer-NH₂ membranes

Spacers	Spacer length	Diamine loading mmol/g	Diamine DS	PPIX loading μmol/g	PPIX DS	Conjugated photosensitizer
Ethylenediamine	4 atoms	0.389 ± 0.058	0.065	4.0 ± 0.3	0.0007	BC-EDA-PPIX
1,2-bis(2-aminoethoxy)ethane	10 atoms	1.775 ± 0.087	0.391	13.0 ± 0.9	0.0021	BC-10-PPIX
1,4-bis(3-aminopropoxy)butane	14 atoms	0.425 ± 0.062	0.075	6.0 ± 0.5	0.0010	BC-14-PPIX

to a higher degree of protonation in acidic media (Zhou et al. 2009). To measure the PPIX loading values, the BC-spacer-PPIX membranes were metallated with zinc as described in the Supporting Information (Sharp et al. 1998), and then ICP-MS was utilized to determine the level of zinc which would equal the level of PPIX present. The values of conjugated PPIX were about 4.0, 13.0 and 6.0 μmol/g for the BC-EDA-PPIX, BC-10-PPIX and BC-14-PPIX, respectively, corresponding to DS values of 0.0007, 0.0021, and 0.0010 (Table 1). These values are on a par with our previous work on porphyrin-cellulose conjugates that had porphyrin loading values of ∼ 3.5 to 33 μmol/g (Carpenter et al. 2015), and demonstrate that the diamine spacer covalent strategy employed here is equivalent to the Cu-catalyzed alkyne azide cycloaddition reaction used in that earlier work.

Resonance Raman spectroscopic studies

Resonance Raman spectroscopy was employed to further characterize the success of the N,N'-carbonyldiimidazole-mediated grafting of PPIX onto the surface of the BC-spacer-NH$_2$ membranes. For the BC-10-PPIX membrane, the Raman spectrum exhibited two new peaks, ∼ 1580 and ∼ 1330 cm^{-1}, which were attributed to the stretching vibrations of the vinyl groups and pyrrole rings, respectively, of the PPIX macrocycle (Jhonsi et al. 2017). PPIX itself exhibited these characteristic peaks, whereas no such features were observed in the spectrum of BC-10-NH$_2$, again consistent with the successful grafting of PPIX onto the nanofibrous OBC membranes.

XPS characterization

XPS spectra were acquired to gain further insight into the surface functional groups and elemental states of the modified membranes. Figure 2 depicts the survey scans of BC-10-NH$_2$ (panel c) and BC-10-PPIX (panel d). Both surfaces showed three apparent peaks centered at 284.8, 399.4 and 532.4 eV corresponding to C 1 s, N 1 s and O 1 s, respectively. The peak associated with N 1 s of BC-10-PPIX was more intense than that of BC-10-NH$_2$, which further confirmed the successful immobilization of PPIX onto the aminated BC membrane. In agreement with the elemental analysis, Fig. 3 illustrates the high-

resolution spectra of C 1 s and N 1 s for BC-10-NH$_2$ and BC-10-PPIX. For the aminated BC-10-NH$_2$ membrane, the C 1 s spectrum was divided into four peaks at 284.7, 285.5, 286.4 and 289.0 eV corresponding to C–C, C–N, C–O and C=O (Lv et al. 2017), respectively, and the N 1 s spectrum was fit to three peaks at 399.5, 399.9 and 402.1 eV corresponding to C–N–C, N–H and C–NH$_3^+$ (Le et al. 2013). For the BC-10-PPIX membrane, an additional peak at 284.eV associated with C = C in the C 1 s spectrum was observed, whereas the N 1 s spectrum exhibited a new peak at 399.3 eV attributed to N=C (Monier et al. 2016). Slight shifts of the other peaks (in comparison to BC-10-NH$_2$) were attributed to the porphyrin units (Zhao et al. 2017). Again, these spectra confirmed the successful grafting of PPIX onto the aminated BC surface.

Photophysical properties

The photophysical properties of the PPIX photosensitizer when grafted on the surface of BC membranes were analyzed by diffuse reflectance UV–Vis (DRUV) and fluorescence emission spectroscopies. For these studies, PPIX in DMSO solution was used as a comparative reference. As shown in Fig. 4a, the DRUV spectrum of BC-10-PPIX exhibited a characteristic Soret band at 405 nm and Q bands between 500 and 700 nm, with both the absorption features and their relative intensities matching well with the parent PPIX photosensitizer in DMSO solution (Natarajan and Raja 2004). The presence of a 'fifth Q band' of free PPIX at 668 nm is likely due to the combination of solvent effects and a high solute concentration (Colpa and Fraaije 2016). The broadened Soret band of the supported BC-10-PPIX was primarily attributed to exciton coupling between chromophores being enhanced in the solid state (Isago 2015), as well as to the porphyrin π-electron interaction with the surface hydroxyl groups of the bacterial cellulose (Ringot et al. 2011). Fluorescence spectroscopy further revealed a high degree of similarly between the grafted PPIX in BC-10-PPIX and PPIX in DMSO solution: when excited at 400 nm, the BC-10-PPIX membrane exhibited a strong emission band at 632 nm along with an additional weak emission band at 678 nm, similar to those observed for free PPIX (Fig. 4b). The slight blue shift of supported PPIX (vs. solution) can be attributed to the differences in the

Fig. 3 C 1 s XPS of **a** BC-10-NH$_2$ and **c** BC-10-PPIX, and N 1 s XPS of **b** BC-10-NH$_2$ and **d** BC-10-PPIX

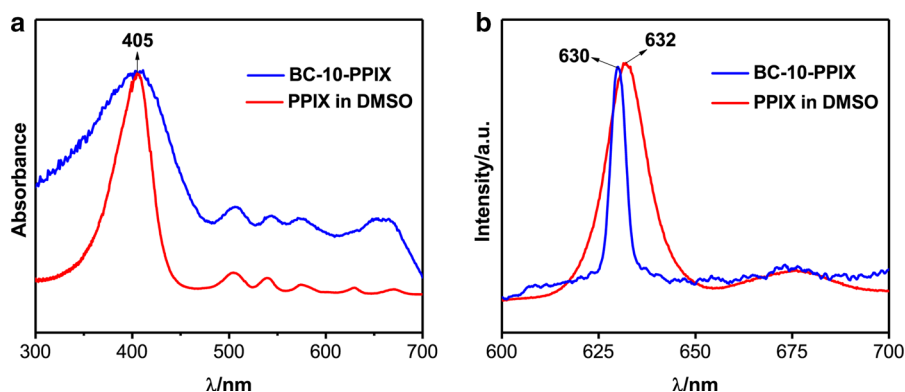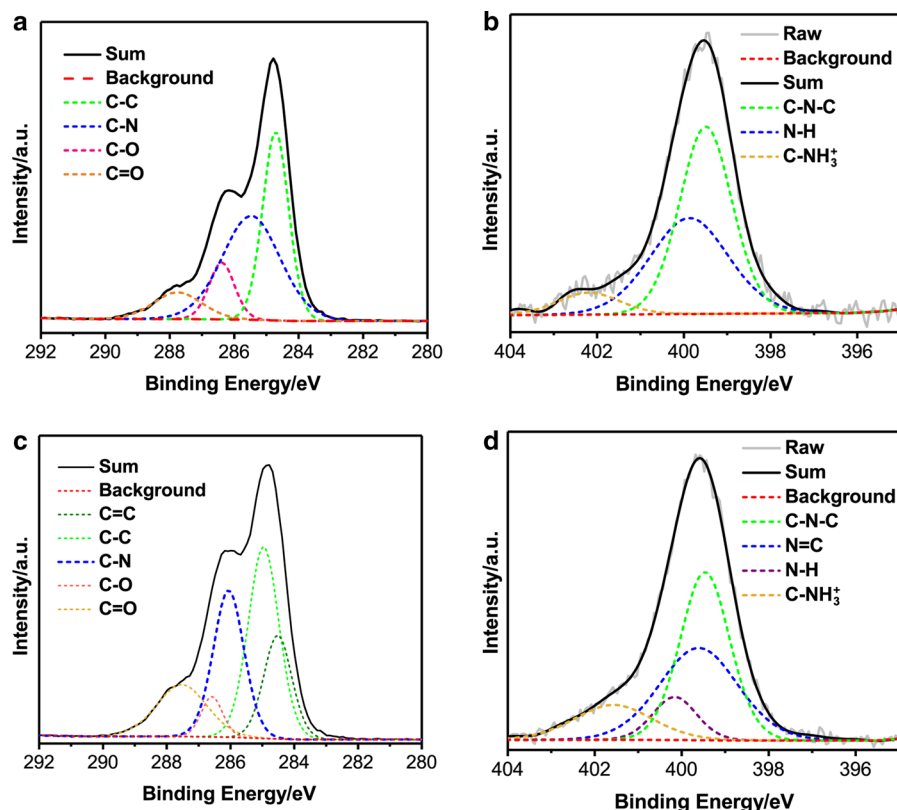**Fig. 4** Absorption (**a**) and fluorescence emission (**b**, $\lambda_{ex} = 400$ nm) spectra of BC-10-PPIX (blue) and PPIX in DMSO solution (red). (Color figure online)

local environment (Carpenter et al. 2015), however two possibilities exist for the narrowing of the emission band in the solid state: (1) the increased constraint in the solid state limits the conformational changes that accompany relaxation to the PPIX ground state (Tirapattur et al. 2003), and (2) non-radiative energy transfer from PPIX fluorophores of higher energy to some of lower energy can occur owing to the close interaction of the PPIX molecules

on the material (Vu et al. 2009). While it is well known that the aggregation of porphyrin chromophores causes fluorescence quenching [which both decreases the efficiency of photosensitization and lowers the aPDI efficacy of the resulting materials (Ogi et al. 2005)], the formation of PPIX aggregates is likely circumvented here through their covalent attachment to the backbone of bacterial cellulose. Taken together, the absorption and emission spectra indicate that the

BC-spacer-PPIX nanofibrous membranes retained the typical photophysical properties of the PPIX chromophore (Lv et al. 2010).

Thermal gravimetric analysis

Thermal gravimetric analysis was performed on pristine BC and BC-spacer-PPIX membranes to gain an understanding of the thermal stability of the prepared materials (Fig. 5). In the first stage up to 100 °C, a minor initial weight loss observed among all membranes was attributed to the loss of water. For the pristine BC membrane, the onset of decomposition started at about 230 °C, with substantial mass reduction only observed above 300 °C. However, the modified BC membranes exhibited two steps of decomposition: the onset of the first decomposition step for the BC-10-PPIX membrane started with a minor mass reduction at about 200 °C, followed by a major weight loss when the temperature was above 280 °C. BC-EDA-PPIX and BC-14-PPIX membranes exhibited similar curves. When compared to pristine BC, we surmise that the lower temperatures for the decomposition of the BC-spacer-PPIX membranes is likely due to the opening of the glucopyranose rings and the breaking of ordered packing that occur during the periodate oxidation process (Kim et al. 2000). Finally, it was noted that the BC-spacer-PPIX membranes yielded more residue than the pristine BC membrane, likely attributed to the grafting of spacers and subsequent PPIX: during the thermal degradation
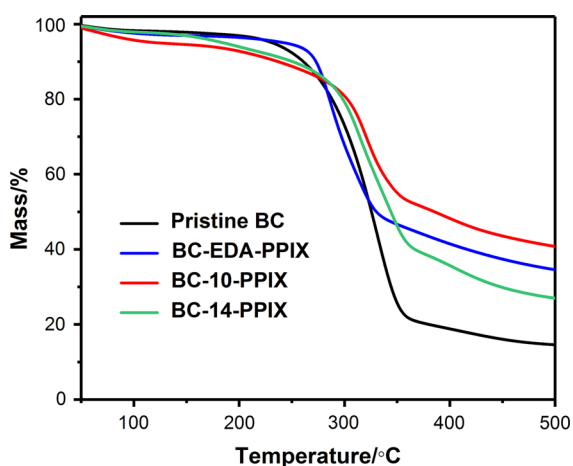

Fig. 5 Thermal gravimetric analysis of pristine BC (red), BC-EDA-PPIX (blue), BC-10-PPIX (yellow) and BC-14-PPIX (green) membranes. (Color figure online)

of the modified membranes under inert atmosphere and at high temperature (above 400 °C), N-containing heterocyclic compounds generate residues from cyclization (Brebu et al. 2000).

Photosensitization of external substrates and model bacteria

Photo-oxidation of external substrates

To compare the photodynamic activity of the BC-spacer-PPIX membranes, a known (Mosinger and Mosinger 1995) acceptor of $^1O_2$ and model substrate, potassium iodide, was used. Oxidation of I^- yielding I_3^- leads to an observable colorimetric assay (Fig. 6a), for which it has been previously shown that the photogenerated concentration of I_3^- is directly proportional to the concentration of $^1O_2$ in an oxygen saturated solution (Henke et al. 2014). As such, the relative photo-oxidation efficacy (PE) of each sample was calculated as the slope of the dependence of absorbance at 287 nm on illumination time. Under identical illumination conditions, the absorbance curve of the BC-10-PPIX membrane exhibited a significantly higher slope than that of either BC-EDA-PPIX or BC-14-PPIX, and is consistent with the higher diamine loading, and consequently PPIX loading, of the 1,2-bis(2-aminoethoxy)ethane aminated BC membrane (see Sect. 3.2.1 and Table 1). Moreover, the similar slopes observed for BC-EDA-PPIX and BC-14-PPIX were also consistent with their similar (within error) loading. As expected, no I_3^- was detected in the dark or upon illumination of the PPIX-free BC membrane.

Photoinactivation of S. aureus and E. coli

In vitro aPDI studies employing the PPIX supported BC membranes were performed using a Xenon lamp (20 cm, 30 min, $\lambda \geq 420$ nm). The antibacterial efficiencies of the samples represented in Fig. 7 were consistent with their ability to oxidize I^- in aqueous solution: upon illumination, *E. coli* was photoinactivated by BC-EDA-PPIX to 77.16% reduction in CFU/mL (~ 0.5 log units), by BC-10-PPIX to 99.999% reduction (5 log units), and by BC-14-PPIX to 68.33% reduction (Fig. 7a). By contrast, under the same illumination conditions no photodynamic inactivation was observed for the pristine BC membrane (PPIX-

Fig. 6 a UV–Vis spectra of KI in oxygen-saturated aqueous solution as photo-oxidized by BC-10-PPIX and **b** the absorbance at 287 nm as a function of continuous illumination with visible light for a 3 mL oxygen-saturated aqueous solution of 0.05 M I$^-$ containing the BC-spacer-PPIX membranes
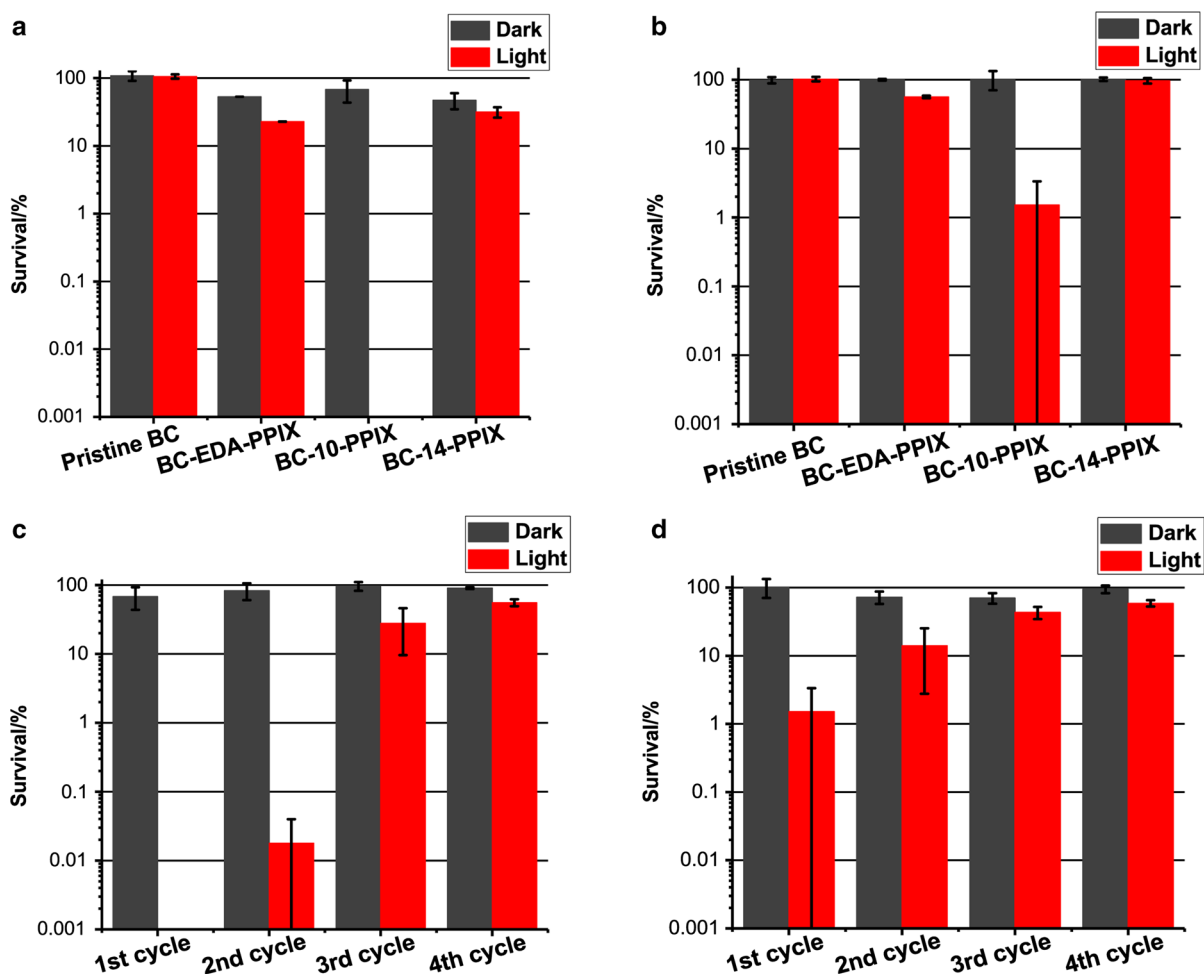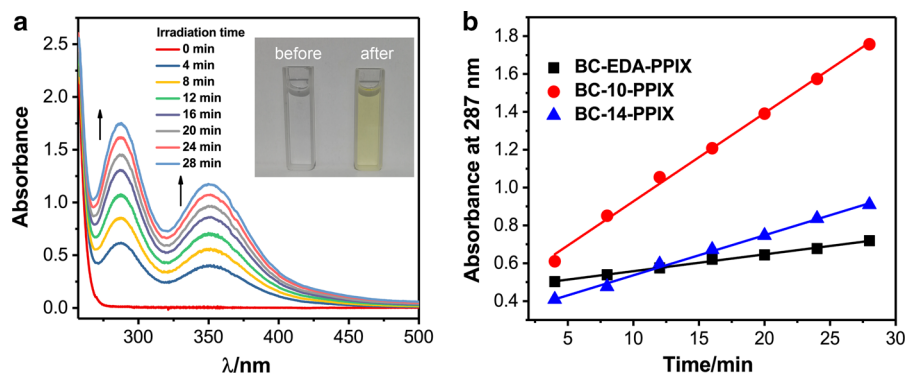

Fig. 7 Photodynamic inactivation using BC-spacer-PPIX membranes of **a** *E. coli* and **b** *S. aureus*. Reusability studies of BC-10-PPIX for 1-4 aPDI cycles against **c** *E. coli* and **d** *S. aureus*

free control), demonstrating the necessity of the PPIX photosensitizer for bacterial inactivation. *S. aureus* was inactivated by 98.50% ($\sim$ 1.5 log units reduction in CFU/mL) by the most effective photosensitizing sample, BC-10-PPIX (Fig. 7b), with lower killing efficiencies seen for the other samples. Overall, we

observed that *E. coli* was much more susceptible to photodynamic inactivation than *S. aureus* with the BC-spacer-PPIX membranes developed here.

Although aPDI is commonly more effective against Gram-positive strains, here we observed that the PPIX-grafted BC membranes exhibited a higher degree of photodynamic inactivation against *E. coli*. EPR analysis of BC-10-PPIX (Figure S2 and Fig. 8a) demonstrated that $^1O_2$ (Type II) was the reactive oxygen species (ROS) that led to the observed bacterial photodynamic inactivation in Fig. 7, so the differential inactivation between *E. coli* and *S. aureus* must be rationalized within the context of this biocidal agent. Two possibilities exist: (1) the presence of lipopolysaccharides and teichoic acids in *E. coli* and *S. aureus*, respectively, confer an overall negative charge to these bacteria. Owing to the incomplete grafting of PPIX onto the aminated BC surface, we surmise that the free primary amine groups on BC-spacer-NH$_2$ would form –NH$_3^+$ in buffer that would result in a positively charged surface (Mehta and Zydney 2008), such that negatively charged bacteria would adhere onto the supported surface (Fig. 8b). As such, the difference in zeta-potential between *E. coli* (− 49 mV) and *S. aureus* (− 31.7 mV) would lead to a stronger attraction of *E. coli* to the surface (Kłodzińska et al. 2010), bringing it in closer proximity to the photosensitizers and the site of $^1O_2$ formation, leading to higher photodynamic inactivation. Alternatively, (2) *S. aureus* has been shown to form grape-like clusters (Koyama et al. 1977), and such clustering of the bacteria (where inner bacteria are protected) may act as a barrier against singlet oxygen. Such differential photodynamic activity that favors *E. coli* inactivation over that of *S. aureus* has

not been observed previously with our other cellulose-porphyrin conjugates (Carpenter et al. 2012, 2015), likely owing to the use of cationic photosensitizers in those studies.

To further explore the durability of these antibacterial materials, BC-10-PPIX was repeatedly used for several cycles, and after each cycle, the membrane was washed with 75% ethanol and then air-dried at room temperature prior to the next assay. A gradual decrease of the antibacterial efficacy was observed for *E. coli*, with the aPDI efficiency reduced from the original 99.999% to 99.98% (2nd cycle), 72.14% (3rd cycle) and to 44.55% for the final cycle (Fig. 7c). Photodynamic inactivation of *S. aureus* also exhibited a similar situation, albeit with lower efficiencies (Fig. 7d). It is generally accepted that photosensitizers immobilized onto polymer scaffolds via a covalent attachment are more stable than those immobilized from non-covalent methods (electrostatic attachment, surface coating, physical blending, and/or interior encapsulation), with covalent attachments yielding more desirable photodynamic properties (Spagnul et al. 2015). Here, our results demonstrated lowered efficiencies when the PPIX-supported BC membranes were re-used, which could be interpreted in light of two key factors: (1) photobleaching of the supported PPIX and (2) accumulation of bacteria onto the supported BC surface after each antibacterial cycle. Protoporphyrin IX itself undergoes photo-oxidation in the presence of molecular oxygen, with the generated singlet oxygen attacking the ground-state porphyrin (Cox and Whitten 1982), resulting in unavoidable photobleaching. This likely played a key role in decreased killing efficiency of both bacterial strains studied. Furthermore, Figure S4 illustrates the SEM image of the BC-

Fig. 8 **a** EPR spectra in D$_2$O acquired after illumination of BC-10-PPIX in the presence of TEMPONE (red), or in the presence of TEMPONE and the singlet oxygen quencher DABCO (blue); **b** mechanism of photodynamic inactivation against G$^-$ bacteria (*E. coli*). (Color figure online)
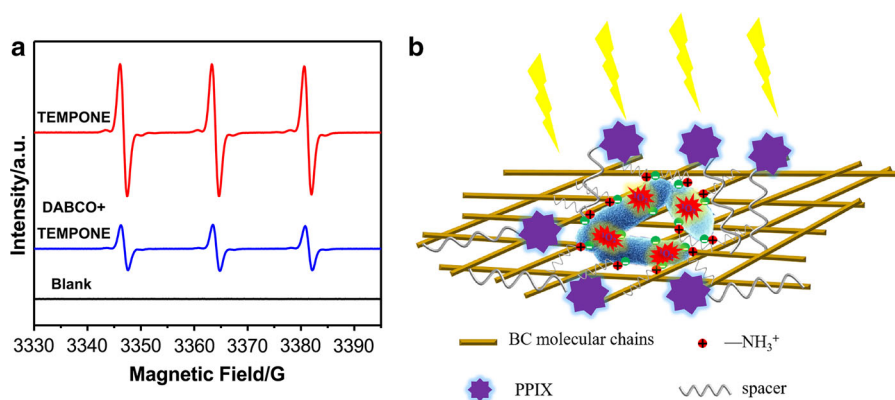
10-PPIX membrane after one cycle of an aPDI assay against *E. coli*. From this image, it is clear that the rod-shaped bacteria adhered on the surface in large clumps. Although the BC-10-PPIX was washed with 75% ethanol, this was apparently not sufficient to dislodge the *E. coli* from the BC-10-PPIX surface, leading to an accumulation of the bacteria that would prevent *E. coli* from the next assay from interacting with surface-located PPIX, and thereby leading to the decreased photodynamic inactivation efficacy observed in Fig. 7.

Conclusions

This work employs a naturally produced nanopolymer, bacterial cellulose (BC), to immobilize the neutral protoporphyrin IX (PPIX) using diamine spacer arms with different chain lengths. In support of our hypothesis, the results demonstrated that the chain length plays a critical role in photosensitizer loading, with the ideal length unit here being the 1,2-bis(2-aminoethoxy)ethane diamine spacer. Antibacterial efficacy was evaluated against both G^+ (*S. aureus*) and G^- (*E. coli*) bacteria. Although aPDI is commonly more effective against Gram-positive strains, here we observed that the PPIX-grafted BC membranes exhibited a higher degree of photodynamic inactivation against *E. coli*, which can be attributed to either the difference in zeta-potential between the two bacteria with respect to the positively charged BC nanosurface, or the higher propensity for *S. aureus* to cluster into aggregates, thereby hindering $^1O_2$ from inactivating the pathogen. Finally, the studies performed here show that bacterial cellulose, with its high specific surface area and hydrophilicity, is a viable biopolymer for use in antimicrobial photodynamic inactivation. Though the reusability of the as-fabricated materials needs to be further enhanced, possibly by employing alternative cleaning procedures or through additional surface modifications, this work provides a potent strategy for the efficient photodynamic inactivation of G^- bacteria using the combination of naturally-derived photosensitizers and biopolymers, both of which provide 'green' alternatives for the next generation of antimicrobial materials.

References

Abrahamse H, Hamblin MR (2016) New photosensitizers for photodynamic therapy. Biochem J 473:347–364

Brebu M, Uddin MA, Muto A, Sakata Y, Vasile C (2000) Composition of nitrogen-containing compounds in oil obtained from acrylonitrile-butadiene-styrene thermal degradation. Energy Fuels 14:920–928. https://doi.org/10.1021/ef000018v

Carpenter BL, Feese E, Sadeghifar H, Argyropoulos DS, Ghiladi RA (2012) Porphyrin-cellulose nanocrystals: a photobactericidal material that exhibits broad spectrum antimicrobial activity. Photochem Photobiol 88:527–536

Carpenter BL et al (2015) Synthesis, characterization, and antimicrobial efficacy of photomicrobicidal cellulose paper. Biomacromolecules 16:2482–2492. https://doi.org/10.1021/acs.biomac.5b00758

Castriciano MA et al (2017) Poly (carboxylic acid)-cyclodextrin/anionic porphyrin finished fabrics as photosensitizer releasers for antimicrobial photodynamic therapy. Biomacromol 18:1134–1144

Colpa DI, Fraaije MW (2016) High overexpression of dye decolorizing peroxidase TfuDyP leads to the incorporation of heme precursor protoporphyrin IX. J Mol Catal B Enzym 134:372–377. https://doi.org/10.1016/j.molcatb.2016.08.017

Cox GS, Whitten DG (1982) Mechanisms for the photooxidation of protoporphyrin IX in solution. J Am Chem Soc 104:516–521

Dahl T, RobertMiddenand W, Hartman P (1987) Pure singlet oxygen cytotoxicity for bacteria. Photochem Photobiol 46:345–352

Fernandes SC, Oliveira L, Freire CS, Silvestre AJ, Neto CP, Gandini A, Desbriéres J (2009) Novel transparent nanocomposite films based on chitosan and bacterial cellulose. Green Chem 11:2023–2029

Gottenbos B, van der Mei HC, Klatter F, Grijpma DW, Feijen J, Nieuwenhuis P, Busscher HJ (2003) Positively charged biomaterials exert antimicrobial effects on gram-negative bacilli in rats. Biomaterials 24:2707–2710

Henke P, Kozak H, Artemenko A, Kubát P, Forstová J, Jí Mosinger (2014) Superhydrophilic polystyrene nanofiber materials generating O₂ (1Δg): postprocessing surface modifications toward efficient antibacterial effect. ACS Appl Mater Interfaces 6:13007–13014

Isago H (2015) Optical spectra of phthalocyanines and related compounds. Springer, Berlin

Jhonsi MA, Nithya C, Kathiravan A (2017) Unravel the interaction of protoporphyrin IX with reduced graphene oxide by vital spectroscopic techniques. Spectrochim Acta A Mol Biomol Spectrosc 178:86–93. https://doi.org/10.1016/j.saa.2017.01.059

Dolanský J, Henke P, Kubát P, Fraix A, Sortino S, Mosinger J (2015) Polystyrene nanofiber materials for visible-light-driven dual antibacterial action via simultaneous photogeneration of NO and O$_2$ ($^1\Delta_g$). ACS Appl Mater Interfaces 7:22980–22989

Johnson BJ et al (2016) Porphyrin-modified antimicrobial peptide indicators for detection of bacteria. Sens Bio Sens Res 8:1–7. https://doi.org/10.1016/j.sbsr.2016.02.005

Jori G, Camerin M, Soncin M et al (2011) Antimicrobial photodynamic therapy: basic principles. In: Hamblin MR, Jori G (eds) Photodynamic inactivation of microbial pathogens: Medical and environmental applications. The Royal Sociey of Chemistry, Cambridge, pp 1–18

Kim U-J, Kuga S, Wada M, Okano T, Kondo T (2000) Periodate oxidation of crystalline cellulose. Biomacromolecules 1:488–492. https://doi.org/10.1021/bm0000337

Kłodzińska E, Szumski M, Dziubakiewicz E, Hrynkiewicz K, Skwarek E, Janusz W, Buszewski B (2010) Effect of zeta potential value on bacterial behavior during electrophoretic separation. Electrophoresis 31:1590–1596

Koyama T, Yamada M, Matsuhashi M (1977) Formation of regular packets of *Staphylococcus aureus* cells. J Bacteriol 129:1518–1523

Krouit M, Granet R, Krausz P (2009) Photobactericidal films from porphyrins grafted to alkylated cellulose—synthesis and bactericidal properties. Eur Polym J 45:1250–1259. https://doi.org/10.1016/j.eurpolymj.2008.11.036

Le Y, Guo D, Cheng B, Yu J (2013) Bio-template-assisted synthesis of hierarchically hollow SiO$_2$ microtubes and their enhanced formaldehyde adsorption performance. Appl Surf Sci 274:110–116

Li H, Wu B, Mu C, Lin W (2011) Concomitant degradation in periodate oxidation of carboxymethyl cellulose. Carbohydr Polym 84:881–886. https://doi.org/10.1016/j.carbpol.2010.12.026

Li G, Nandgaonkar AG, Wang Q, Zhang J, Krause WE, Wei Q, Lucia LA (2017) Laccase-immobilized bacterial cellulose/TiO$_2$ functionalized composite membranes: evaluation for photo- and bio-catalytic dye degradation. J Membr Sci 525:89–98. https://doi.org/10.1016/j.memsci.2016.10.033

Liu F, Soh Yan Ni A, Lim Y, Mohanram H, Bhattacharjya S, Xing B (2012) Lipopolysaccharide neutralizing peptide–porphyrin conjugates for effective photoinactivation and intracellular imaging of gram-negative bacteria strains. Bioconj Chem 23:1639–1647. https://doi.org/10.1021/bc300203d

Lv Y-Y, Wu J, Xu Z-K (2010) Colorimetric and fluorescent sensor constructing from the nanofibrous membrane of porphyrinated polyimide for the detection of hydrogen chloride gas. Sens Actuators B Chem 148:233–239. https://doi.org/10.1016/j.snb.2010.05.029

Lv P, Feng Q, Wang Q, Li G, Li D, Wei Q (2016) Biosynthesis of bacterial cellulose/carboxylic multi-walled carbon nanotubes for enzymatic biofuel cell application. Materials 9:183

Lv P et al (2017) Self-assembly of nitrogen-doped carbon dots anchored on bacterial cellulose and their application in iron ion detection. Carbohydr Polym 172:93–101

Mehta A, Zydney AL (2008) Effect of spacer arm length on the performance of charge-modified ultrafiltration membranes. J Membr Sci 313:304–314. https://doi.org/10.1016/j.memsci.2008.01.014

Moan J, Wold E (1979) Detection of singlet oxygen production by ESR. Nature 279:450–451. https://doi.org/10.1038/279450a0

Monier M, Abdel-Latif DA, Abou El-Reash YG (2016) Ion-imprinted modified chitosan resin for selective removal of Pd(II) ions. J Colloid Interface Sci 469:344–354. https://doi.org/10.1016/j.jcis.2016.01.074

Mosinger J, Mosinger B (1995) Photodynamic sensitizers assay: rapid and sensitive iodometric measurement. Experientia 51:106–109

Natarajan P, Raja C (2004) Studies on interpolymer self-organisation behaviour of protoporphyrin IX bound poly(-carboxylic acid)s with complimentary polymers by means of fluorescence techniques. Eur Polym J 40:2291–2303. https://doi.org/10.1016/j.eurpolymj.2004.06.003

Ogi T, Kinoshita R, Ito S (2005) Spectroscopic and optical characterization of porphyrin chromophores incorporated into ultrathin polyimide films. J Colloid Interface Sci 286:280–287. https://doi.org/10.1016/j.jcis.2005.01.001

Onem H, Nadaroglu H (2014) Preparation and properties of purified phytase from oakbug milkcap (*Lactarius quietus*) immobilised on coated chitosan with iron nano particles and investigation of its usability in food industry. J Food Nutr Res 2:938–945

Rahimi R, Fayyaz F, Rassa M (2016) The study of cellulosic fabrics impregnated with porphyrin compounds for use as photo-bactericidal polymers. Mater Sci Eng C 59:661–668. https://doi.org/10.1016/j.msec.2015.10.067

Ringot C et al (2011) Triazinyl porphyrin-based photoactive cotton fabrics: preparation, characterization, and antibacterial activity. Biomacromolecules 12:1716–1723. https://doi.org/10.1021/bm200082d

Sharp RE, Diers JR, Bocian DF, Dutton PL (1998) Differential binding of iron (III) and zinc (II) protoporphyrin IX to synthetic four-helix bundles. J Am Chem Soc 120:7103–7104

Shrestha A, Hamblin MR, Kishen A (2014) Photoactivated rose bengal functionalized chitosan nanoparticles produce antibacterial/biofilm activity and stabilize dentin-collagen. Nanomed Nanotechnol Biol Med 10:491–501. https://doi.org/10.1016/j.nano.2013.10.010

Spagnul C, Turner LC, Boyle RW (2015) Immobilized photosensitizers for antimicrobial applications. J Photochem Photobiol B 150:11–30

Stanley SL, Scholle F, Zhu J, Lu Y, Zhang X, Situ X, Ghiladi RA (2016) Photosensitizer-embedded polyacrylonitrile nanofibers as antimicrobial non-woven textile. Nanomaterials 6:77

Tirapattur S, Belletête M, Drolet N, Leclerc M, Durocher G (2003) Steady-state and time-resolved studies of 2, 7-carbazole-based conjugated polymers in solution and as thin films: determination of their solid state fluorescence quantum efficiencies. Chem Phys Lett 370:799–804

Vallapa N, Wiarachai O, Thongchul N, Pan J, Tangpasuthadol V, Kiatkamjornwong S, Hoven VP (2011) Enhancing antibacterial activity of chitosan surface by heterogeneous quaternization. CarbohydR Polym 83:868–875. https://doi.org/10.1016/j.carbpol.2010.08.075

Vu TT et al (2009) New hindered BODIPY derivatives: solution and amorphous state fluorescence properties. J Phys Chem C 113:11844–11855

Wen X, Zhang X, Szewczyk G, El-Hussein A, Huang Y-Y, Sarna T, Hamblin MR (2017) Potassium iodide potentiates antimicrobial photodynamic inactivation mediated by Rose Bengal: in vitro and in vivo studies. AAC 61:00467–00417

Wu J, Meredith JC (2014) Assembly of Chitin Nanofibers into Porous Biomimetic Structures via Freeze Drying. ACS Macro Lett 3:185–190. https://doi.org/10.1021/mz400543f

Zhao G et al (2017) Co-porphyrin/carbon nitride hybrids for improved photocatalytic CO_2 reduction under visible light. Appl Catal B 200:141–149

Zhou Z, Xiao Y, Hatton TA, Chung T-S (2009) Effects of spacer arm length and benzoation on enantioseparation performance of β-cyclodextrin functionalized cellulose membranes. J Membr Sci 339:21–27. https://doi.org/10.1016/j.memsci.2009.04.015

Zhu J, Sun G (2012) Preparation and photo-oxidative functions of poly(ethylene-co-methacrylic acid) (PE-co-MAA) nanofibrous membrane supported porphyrins. J Mater Chem 22:10581–10588. https://doi.org/10.1039/C2JM16703D